A multi-sensor and multi-temporal remote-sensing approach to detect land cover change dynamics in heterogeneous urban landscapes

Nadja Kabisch [1,2*], Peter Selsam [3], Toralf Kirsten[4,5], Angela Lausch [6,1], Jan Bumberger[7]

1 Humboldt-Universität zu Berlin, Department of Geography, Rudower Chaussee 16, 12489 Berlin, Germany, Germany
2 Helmholtz Centre for Environmental Research – UFZ, Department of Urban and Environmental Sociology, Permoserstraße 15, 04318 Leipzig, Germany
3 codematix GmbH, Felsbachstrasse 5/7, 07745 Jena, Germany
4 LIFE Research Centre for Civilization Diseases, University of Leipzig, Philipp-Rosenthal-Straße 27, 04103 Leipzig, Germany
5 University of Applied Sciences Mittweida, Faculty Applied Computer Sciences and Biosciences, Am Technikumplatz 17, 09648 Mittweida, Germany
6 Helmholtz Centre for Environmental Research – UFZ, Department of Computational Landscape Ecology, Permoserstraße 15, 04318 Leipzig, Germany
7 Helmholtz Centre for Environmental Research – UFZ, Department of Monitoring and Exploration Technologies, Permoserstraße 15, 04318 Leipzig, Germany

Correspondance: *nadja.kabisch@geo.hu-berlin.de

Declarations of interest: none.

Abstract

With global changes such as climate change and urbanization, land cover is prone to changing rapidly in cities around the globe. Urban management and planning is challenged with development pressure to house increasing numbers of people. Most up-to date continuous land use and land cover change data are needed to make informed decisions on where to develop new residential areas while ensuring sufficient open and green spaces for a sustainable urban development. Optical remote sensing data provide important information to detect changes in heterogeneous urban landscapes over long time periods in contrast to conventional approaches such as cadastral and construction data.

However, data from individual sensors may fail to provide useful images in the required temporal density, which is particularly the case in mid-latitudes due to relatively abundant cloud coverage. Furthermore, the data of a single sensor may be unavailable for an extended period of time or to the public at no cost. In this paper, we present an integrated, standardized approach that aims at combining remote sensing data in a high resolution that are provided by different sensors, are publicly available for a long-term period of more than ten years (2005-2017) and provide a high temporal resolution if combined. This multi-sensor and multi-temporal approach detects urban land cover changes within the highly dynamic city of Leipzig, Germany as a case. Landsat, Sentinel and RapidEye data are combined in a robust and normalized procedure to offset the variation and disturbances of different sensor characteristics. To apply the approach for detecting land cover changes, the Normalized Difference Vegetation Index (NDVI) is calculated and transferred into a classified NDVI (Classified Vegetation Cover – CVC). Small scale vegetation development in heterogeneous complex areas of a European compact city are highlighted. Results of this procedure show successfully that the presented approach is applicable with divers sensors' combinations for a longer time period and thus, provides an option for urban planning to update their land use and land cover information timely and on a small scale when using publicly available no cost data.

Keywords: Greenness; NDVI, Classified Vegetation Cover (CVC); remote sensing, urban areas, Leipzig, new approach; multi-sensor, multi-temporal

1 Introduction

Global changes such as climate change and urbanization are driving land use and land cover changes in cities on a global scale. Consequently, processes related to climate change are responsible for the establishment of alien plant species, the degradation of species habitats and biodiversity change, causing increased heat and drought impacts and water scarcity with related effects on vegetation (Carter, 2011). In addition, the increase in the number of people in urban areas all around the world is threatening ecosystems as urbanization is accompanied by massive soil sealing, the densification of built-up areas and the related loss and degradation of urban green spaces (Kabisch et al. 2017).

Faced with the pressure of accommodating an increasing number of people while at the same time maintaining urban green spaces (Feltynowski et al., 2017; Frantzeskaki and Kabisch, 2016), urban planning requires detailed land use and land cover information with a high temporal and spatial resolution. The provision of continuous urban Land Use and Land Cover (LULC) change information is, however, exacerbated by insufficient labor, limited time and expertise in local planning departments (Kabisch 2015). The use of optical Remote Sensing (RS) data might be one option to provide continuous information on LULC with high temporal and spatial resolution. In particular, RS data enable a detailed monitoring of LULC information to assess and quantify land development processes from the local to the global scale (Wulder and Coops, 2014) and from short-term (Frazier et al., 2018) to long-term (Tayyebi et al., 2018).

RS data relevant for detecting LULC in urban areas are provided by different sensor systems. Landsat or Sentinel 2 sensors cover large areas with high spatial and temporal resolution. So far, a number of new and updated data policies allow a free access to download data from sensor archives (Wulder and Coops, 2014). They include RS data from sensors like Landsat (Wulder et al., 2008), Sentinel (Drusch et al., 2012) Spot satellite, the IRS-1C, IRS-1D-, or data from Resourcesat-1-Missions, Resourcesat-2 and Cartosat-1 missions. Future satellite missions such as the hyperspectral imager mission EnMAP (Environmental Mapping and Analysis Programme (Guanter et al., 2015)) also intend to follow an Open Data policy soon.

In the context of urban areas, noteworthy are the Landsat archives that were opened in 2008 and provide detailed remote-sensing imagery with a high spatial resolution of 30 meters from the early 1980s (Wulder et al., 2012). The long-term record of Landsat observations and the opening of the data archives without the need to pay for them has led to a number of interdisciplinary studies on change detection of the Earth's surface, e.g. in biodiversity change (Pereira and Cooper, 2006), forest cover changes (Banskota et al., 2014), forest disturbances (Müller et al., 2016), coastline erosion (Fan et al., 2018), the expansion of urban areas (Schetke et al., 2016; Seto and Fragkias, 2005; Small, 2006) or even public health (Dadvand et al., 2012; Gascon et al., 2016).

With the opening of the archives, and the immense number of images now available, (semi) automated algorithms aiming at high spatial-temporal density have been developed recently (Healey et al., 2018; Vázquez-Jiménez et al., 2018). Together, the multitude of available images, as opposed to relying on single cloud-free images, and the newly developed algorithms and available data technologies allow for the creation of seamless imagery suitable for spatial and temporal change LULC detection (Hansen and Loveland, 2012). This opportunity has already been used to assess changes in forest areas to detect forest disturbance (Kennedy et al., 2010; Zhu et al., 2012). However, comparatively less has been undertaken to develop automated and transferable methods for merging images from different sensor types over time to understand LULC in heterogeneous systems of urban areas.

To detect impacts from urbanization on urban LULC change, i.e. densification processes, loss of urban green and open spaces and others, so far RS data from one sensor and single time periods have been used to calculate indicators of land use change. One of the most common indicator used is the Normalized Difference Vegetation Index (NDVI, Pettorelli et al. 2005). The NDVI is used to detect vegetation cover or greenness and conversely to detect soil sealing based on multispectral RS data

(Pettorelli et al., 2005). It is calculated from spectral reflectance measurements in the visible red band (RED) in combination with near-infrared regions (NIR) and is derivable with the equation NDVI = (NIR-RED)/ (NIR+RED) (Myneni et al., 1995; Running, 1990). The NDVI provides normalized values in a range from {−1 to 1}. The NDVI has gained widespread importance for monitoring, quantification and valuation of plant processes, and thus, the spectral bands used for NDVI derivation are integrated into most optical remote sensors. The NDVI shows how relations to Photosynthetically Active Radiation (PAR) and can be used to calculate the net exchange of CO_2 for ecosystems (Alcaraz et al., 2006; Morgan et al., 2016; Wang et al., 2012). It can also be used to assess differences between canopy structures and phenological characteristics (Kim, 2010; Steven et al., 2003; Yin et al., 2012). There has also been significant effort to cross-calibrate different sensors to develop time series on larger scales (Deutscher Wetterdienst - DWD, 2017; Marshall et al., 2016) but continued vegetation index registrations available on global databases are to coarse for urban structure investigations.

With Landsat however, vegetation reflectance values of different sensors turned out to be highly correlated (Brown et al., 2008; Zhang and Roy, 2016) even if sensor specific differences were nonlinear (Myneni et al., 1995). Thus, the NDVI derived from different sensor information might be used to detect small scale densification processes or changes in green space cover even in urban areas. Still, the range of values is different when highly diverse urban land use structures with a high complexity of green vegetation with non-green streets, buildings or bare soil are considered (Gascon et al., 2016).

Detecting LULC information in urban areas comes up with a number of challenges:

- The spatial resolution of sensor based images need to be high enough to differentiate between different structures of urban land use and urban land cover.
- The sensor design should allow meaningful indices such as the NDVI to be calculated. Given the complexity and multidimensionality in urban areas, however, the NDVI may underestimate greenness in urban green spaces (Wellmann et al., 2018).
- Urban regions are highly dynamic areas. Complex urban structures can change over time and within a small period and certainly change over a number of years (Wellmann et al. 2018).
- Satellite programs such as Landsat, Spot or IRS have been providing images for more than 25 years now (RapidEye for 10 years), which may be used to detect the status and changes in structures over time. However, it remains uncertain to which extent the different optical RS data are suitable by comparison for recording heterogeneous, complex and small-scale urban areas.

To address these challenges, in this paper, we present an approach that applies algorithms to normalize and detect change in urban greenness using NDVI and multi-sensor remote sensing data to show how green space is developing in quantity and quality over space and time in a highly dynamic city. In particular, we aim at:

(i) providing a comparative assessment of the data availability, usability and robustness of optical remote sensing data – Landsat 5-8, Sentinel 2 and RapidEye data;

(ii) measuring the mean "greenness" of city districts by means of the NDVI for an entire annual vegetation period and to compare the change in greenness over more than ten years by using public accessible data of medium resolution (at least 30 m); and

(iii) presenting the application of an organized automated and less cost-intensive and less time-consuming data processing chain through remote sensing that is applicable to urban areas, covering a compact investigation period with as many images as possible, which may also be transferable on the global scale.

2. Study area

We use the city of Leipzig, Germany as a case (Figure 1). Leipzig is located in the Free State of Saxony in the floodplains of the rivers Weiße Elster, Pleiße and Parthe. Leipzig covers an area of 297 km² and has a population number of 590,337 (2017), resulting in a population density of 1,988 inhabitants per square kilometer. Leipzig is a compact central European city with a comparatively homogenous architectural structure, such as “Wilhelminian-period” block estates, large prefabricated housing estates, single and detached homes and semi-detached houses.

The city is interesting for us as a case to explore LULC change through RS data because it experienced post-socialist urban structural change after 1989 and has been undergoing a wide urban restructuring process since the year 2000. The population decreased from 530,000 in 1989 to 437,000 in 1998. Population losses led to empty residential properties, ending in house demolitions that produced new spatial patterns such as brownfield sites, demolition corridors and ‘housing islands’. However, population numbers have been exponentially increasing since the year 2000 and the population prognosis suggests an increase in the population up to a total population number of around 700,000 by 2032 (City of Leipzig, 2016). Based on the increasing population numbers and updated population prognosis, the creation of a new urban development concept of the city of Leipzig (SEKo Leipzig 2020) started in 2007 with reference to recommendations of the Free State of Saxony from 2005 (City of Leipzig, 2009). A main aim here has been the maintenance and development of new green and open spaces. Nevertheless, continuing population increases have been resulting in densification processes and new residential development processes currently taking place in the form of building new properties on nearly every available spot in attractive city areas. These processes lead to loss of green but also to the creation of new green spaces through the demolition measures or the re-design of former brownfield sites into newly developed parks. Monitoring green space and new residential developments with RS data can help urban planning updating their development concepts and land cover change maps to make most up to date and informed decisions to where to implement and introduce their sustainable development strategies. To further increase sustainable urban development, currently, the city of Leipzig is planning a new Masterplan 2030 for new green space implementation strategies. The current LULC data for the city is based on information from 2011. Continuously updated LULC information is therefore of importance for the city.

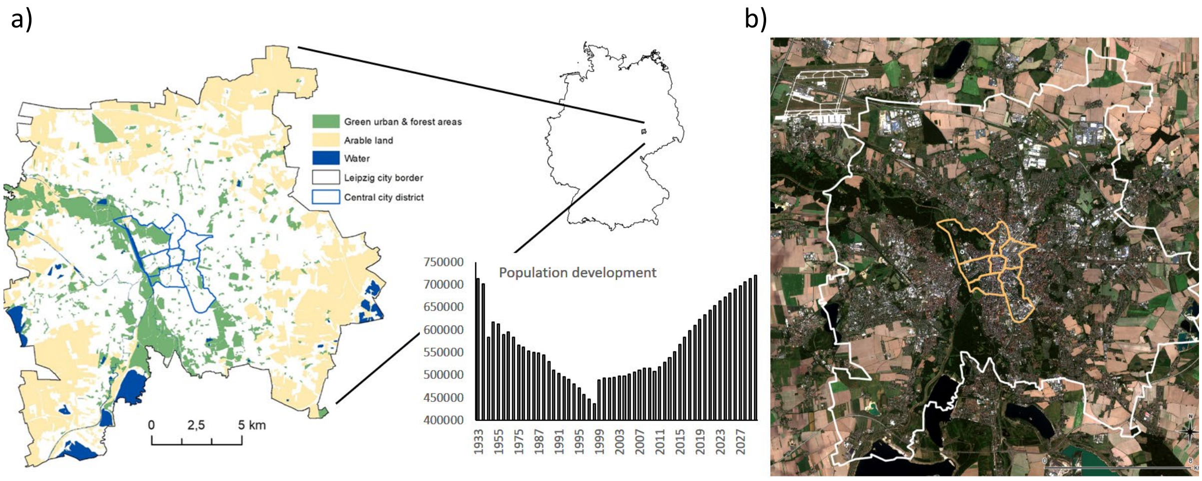

Figure 1: a) Case study city of Leipzig with central inner-city districts (blue line), location of Leipzig in Germany and population development. b) Rapid Eye image of Leipzig in RGB with central inner-city districts (orange line).

3. Methodical approach

To detect green space development over a longer time-period of at least one decade, we followed a structured approach that is shown in detail in Figure 2. Single steps of the approach are explained in sub-chapters below.

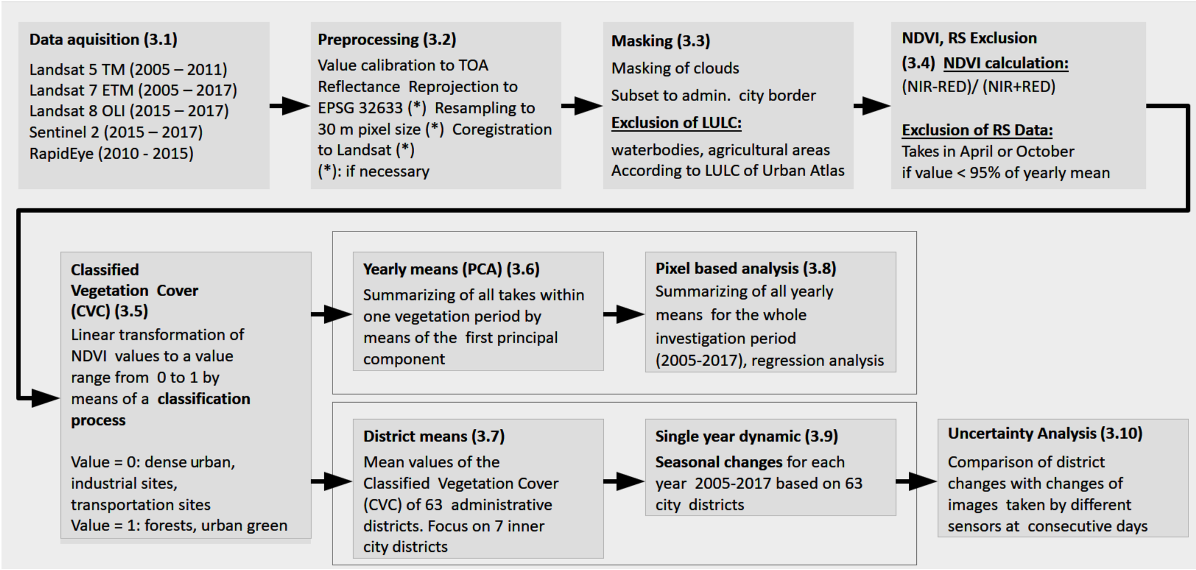

Figure 2: Information flow diagram of the methodological approach.

3.1 Remotely Sensed Data Acquisition

We intended to cover all public available data for the time period 2005 to 2017 (Table 1) from divers sensor types. The period 2005-2017 was chosen because we intended to analyse LULC for at least one recent decade. Further, the new urban development concept for the city of Leipzig started to get developed around that time.

Available satellite images were downloaded from the United States Geological Survey (USGS) Landsat archive (Earth Explorer) and the European Space Agency (ESA) Sentinel archive (Copernicus scihub). The commercial data from the Planet Labs company (order for RapidEye images, Planet, Planet.org) were obtained from a UFZ contract (Tereno Contract nr. 462/703). Image data were provided by the Landsat 5 TM sensor (2005 - 2011), Landsat 7 ETM (2005 - 2017), Landsat 8 OLI (2015 – 2017), Sentinel 2 (2015 – 2017) and RapidEye (2010 - 2015) (see Table 1).

Landsat and Sentinel data are accessible via open access data archives and image acquisition will continue in coming decades. RapidEye is a commercial program and images must be ordered but the system design allows a very high repetition rate (daily off nadir and 5.5 days in nadir position) of a certain place. Cloudless images can be selected by order and compared with the freely available data that show interruptions by clouds in most cases. We limited the image acquisition to the vegetation period (April to October) to assess fully developed vegetation.
Finally, 97 remote sensing scenes from five different sensors were used (see Supplementary Material A for a full list of images). The highest number of images was provided for 2011 and then available for the month of August (Figure 3a and 3b).

Table 1. Remote sensing data used for NDVI calculation by data source (DOI of images in supplement).

Year	Remote Sensing Missions Name	Time period	No of usable images
2005	Landsat 5[1], 7[2]	May – October*	8 takes
2006	Landsat 5, 7	June - September	6 takes
2007	Landsat 5, 7	May - July	3 takes
2008	Landsat 7	June - October	3 takes
2009	Landsat 5,7, RapidEye[5]	April – September	11 takes
2010	Landsat 5,7, RapidEye	April - October	10 takes
2011	Landsat 5, 7, RapidEye	April - September	14 takes
2012	Landsat 7, RapidEye	May - September	5 takes
2013	Landsat 7, 8[3]	June – August	4 takes
2014	Landsat 7, 8	April - September	8 takes
2015	Landsat 7, 8, Sentinel 2[4]	April - October	9 takes
2016	Landsat 7, 8 Sentinel 2	May - September	12 takes
2017	Landsat 7, 8 Sentinel 2	May - October	4 takes

[1]*Landsat 5,* NASA & USGS; Launch date: 1982; revisit time for Europe: 16 day, Type of sensor: - Multi-spectral push broom imager & TIR multi band thermal infrared radiometer/ spectral information: 7 spectral bands (VNIR)-30m, 1 spectral bands (TIR)- 120m; [2]*Landsat 7,* NASA & USGS; Launch date: 1999; revisit time for Europe: 16 day. Type of sensor: - Multi-spectral push broom imager & TIR multi band thermal infrared radiometer/ spectral information: 7 spectral bands (VNIR)-30m, 1 spectral bands (TIR)- 60m, 1 panchromatic band (PAN)-15m; *Landsat 8,* NASA & USGS; Launch date: 2013; revisit time for Europe: 13 day, Type of sensor: - OLI- Imaging multiband spectrometer & TIR multi band thermal infrared radiometer/ spectral information:1 panchromatic band (PAN)-15m, 9 spectral bands (VNIR)-30m, 2 spectral bands (TIR)- 100m; [4] Sentinel-2A/B; two-satellite configuration/ ESA; Launch date: 2015/2016; revisit time for Europe: 5 day, Multi-spectral imaging spectrometer; spectral information: 12 spectral bands; visible and VNIR) – 10m; (VNIR, SWIR) – 20m, (high radiometric resolution, visible -)-60m; [5] RapidEye; PlanetLabs; Launch date: 2008; revisit time for Europe: Daily (off nadir), 5.5 days (at nadir)Type of sensor: Multi-spectral push broom imager /spectral information: 5 spectral bands-5(6.5)m. *for more information, see Supplementary Material A.

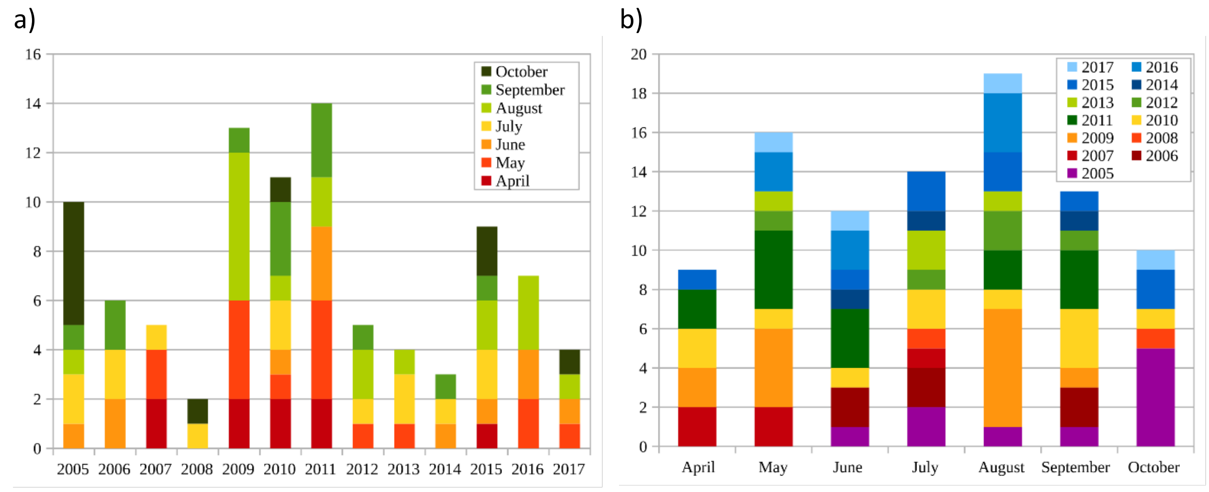

Figure 3. a) Distribution of all remote sensing data 2005-2017, different colors depict the months of the accepted remote sensing data. b) Distribution of all remote sensing data over different months, different colors depict different years.

3.2 Preprocessing

Most of the provided image scenes were projected to zone 33 (EPSG 32633). In all other cases, the subsets were reprojected from EPSG 32632 to EPSG 32633 using the Lanczos algorithm for pixel value interpolation implemented in Quantum GIS version 2.18 (Lanczos, 1950). All image data values (Landsat 5, Landsat 7, Landsat 8, Sentinel 2, RapidEye) were transferred to reflectance according to the providers instructions. Calibration parameters were taken from the image metadata provided by USGS, ESA or Planet Labs (ESA, 2015; NASA, 2017, 2015; PLANET, 2017) respectively. After calibration and reprojection Sentinel and RapidEye image data were resampled to 30m pixel size and co-registered to

Landsat scenes of the same vegetation period using Quantum GIS 2.18. We aimed at integrating all available and usable images for a whole vegetation period for each year regardless of the type of sensor.

3.3 Masking

A number of remotely sensed image data for Central Europe shows clouds but in many cases they cover only small parts of the image. Before calculating the vegetation index, clouds and the shadows of clouds were removed from the image data and set to “NoData”. Landsat data were preselected for a cloud cover of less than 40%. The USGS specification was verified manually as clouds may be very unequally distributed over the whole image. As for USGS data, this verification step was the only one done visually. Landsat image data are provided with a QA-band (Quality Assessment (QA) band) that meets all of our needs to cover clouds and image gaps (stripes) caused by the shutter defect of Landsat 7 (NASA 2017). To mask total cloud cover in Landsat data "high confidence cirrus", "high confidence cloud", "high confidence "shadow" and "secured clouds" were extracted from the binary coded QA band (USGS QA-Tools 2017). The QA-channel simultaneously has different masks in binary code (USGS QA-Tools 2017). A transfer of the code into defined masks is implemented in the ILMS image tool (ILMSimage, Kralisch et al. 2012), which is used in our approach.
Sentinel 2 scenes were selected using a maximum cloud cover of 20%. This differs from the Landsat criteria where a cloud cover of less than 40% was assessed to be sufficient. We decided to accept only Sentinel 2 scenes with a maximum cloud cover of 20% because the cloud cover mask provided by the ESA image product (gml-polygons) proved to be insufficient for our needs. For RapidEye data the use of a cloud mask was not required. In our approach, we used as many image acquisition dates as possible with the mentioned restrictions to cloud cover. Our strategy calls for a careful and well-developed cloud mask in particular, when aiming at high temporal data density.

All of the selected and used images in this study were cut by a 3 km buffer around Leipzig’s administrative city border to cover the city area of Leipzig. The city area of Leipzig includes a considerable amount of agricultural areas and large areas of what used to be open-cast mining areas that have been turned into waterbodies within the last decades. We excluded both, waterbodies and agricultural areas from further investigation, because the "greenness" of waterbodies cannot be quantified by a vegetation index and agricultural land is mostly highly managed with vegetation changes occurring immediately in the vegetation period of interest. Both of these types of LULC were excluded using the land cover classification codes 5000 and 3000 from the European Urban Atlas land cover map provided by the European Environment Agency (European Commission, 2011).

3.4 Normalized difference vegetation index, RS exclusion

The NDVI was used as a basis of all further calculations. The vegetation period may start and end at slightly different dates. We used the NDVI values to get information about fully developed vegetation. The NDVI was calculated by using calibrated standard Top Of Atmosphere (TOA) reflectance values according to the provider instructions (conversion equation is given in Supplementary Material D). We intended to include all available scenes from April to October. Images taken at the first and the last month were excluded from the final analysis if the vegetation was not fully developed or after the fall of leaves had started. To remove outliers, the selection images with the mean of 5% smaller NDVI values than the remaining minimum of that year were excluded. This criterion was applied in 6 out of 103 cases (see Supplementary Material A).

3.5 Classified Vegetation Cover

Classifying the NDVI values was used as a step to assign a biological “meaning” and to get a normalized NDVI product to the values that describe the reflectance and fluorescence of vegetation. The procedure follows a standard classification process where reference areas are defined and linked to values that describe qualities. In this case, only two reference areas were necessary: one for completely sealed areas with no vegetation and the other for those areas completely covered by vegetation. All other qualities are degrees between these two extremes. We did not use standard ground truth training areas to get minimum and maximum values for plant cover but instead used a value frequency histogram of the NDVI for this purpose. In the case of Leipzig, standard reference areas for completely sealed areas and areas with full vegetation cover would have been easily detectable, but with this frequency histogram method, the approach is transferable to other cities.

For the Classified vegetation cover (CVC) NDVI values were given a value between zero (no vegetation cover) and one (dense vegetation cover). The training areas for classification were derived from the actual image data. For this purpose, for every image a value-frequency histogram with 4096 steps was calculated and converted into the summary histogram. The values for 1% and for 99% of the summary histogram were used as typical extreme NDVI values for "no vegetation cover" (equal 0) and "dense vegetation cover" (equal 1). All NDVI values between these extreme values were transformed in a linear fashion range from {0 to 1}. To evaluate the accuracy of the histogram derived masks, the results for 2012 were compared with the Urban Atlas LULC and used for the accuracy test. The mask for "no vegetation cover" is spread between "Continuous Urban", "Industrial & Commercial" and "Traffic", whereas the mask for "closed vegetation cover" is comprised of "Green Urban", "Sports & Leisure" and "Forest" (Supplementary Material B and C). Which means that a “dense vegetation cover” mask is situated completely within Urban Atlas classes of continuous vegetation cover and the “no vegetation cover” mask is completely covered by Urban Atlas classes with highest urban density. Obviously the approach shows high accuracy when comparing with the Urban Atlas classes.

3.6. Yearly Mean Principal Component Analysis (PCA)

NDVI values are often summarized for integration over one vegetation period. To compare different vegetation periods, however, a calculation method is needed that is less sensitive to occasional extreme values. Thus, we used the first principal component to receive a compromise between sum and extreme values. For each year of the investigation period the first principal component for all single takes of one year was calculated and transferred into a yearly NDVI and a Classified Vegetation Cover (CVC) according to the procedure of single takes. The results were taken as summarized values over the year. The result is referred to as “Yearly mean”.

3.7. District means

To compare different administrative districts of Leipzig and follow their development over time, the CVC values were summarized arithmetically on the district level for Leipzig (Leipzig comprises 63 districts) – also called “District means”. District mean values show the development of the vegetation of single districts within one vegetation period (Fig. 4a, b) and over different years (Fig. 5a, b).

3.8. Pixel based analysis (2005-2017)

A pixel based first principal component and regression of all yearly means data was calculated for different years and time periods (2005-2011 and 2012-2017) to show intensity and direction of regional green space and residential developments without the value low pass summarizing necessary caused by the city districts. The regression results of the yearly means emphasis local changes, primarily new buildings (small red dots) and larger areas with newly grown up plants.

3.9. Single year dynamic

For each year the seasonal changes of NDVI and CVC were calculated on the basis of city district means. Based on this results a few images were excluded from further investigation because the vegetation metabolism seemed to be reduced in April and/or October (cf. 3.4).

3.10. Uncertainty Analysis

To check for value differences in CVC caused by the use of different sensors we aimed at comparing images taken at consecutive days by different sensors as an uncertainty analysis. A total of 14 image pairs with daily differences were observed. The daily differences were calculated on the basis of CVC values for 63 city districts in the same way as single year dynamics. The pairs are compared in terms of global differences caused by different sensor properties and local differences caused by changes of vegetation metabolism.

4. Results

The aim of this study was to present a remote-sensing based multi-sensor and multi-temporal approach to detect urban land cover change. In particular, the approach aimed at integrating and combining highly resoluted, publicly available remote sensing data from different sensors for a long-term seamless period of more than one decade (2005-2017). To detect land cover change, a normalized urban greenness algorithm based on the NDVI was used to show changes in the “greenness” of Leipzig’s districts.

4.1 Value changes and the role of CVC

In terms of temporal image coverage, we found 3-10 scenes during one vegetation period per year with sparse or no cloud covers when we merged different sensor types. The combination of different sensor types provided more images and thus more reliable results. This approach of image combination allowed data to be used that showed incomplete coverage caused by clouds or sensor defects.

The NDVI dynamic is illustrated in Figure 4a for seven central inner-city districts for the year 2005. The seven districts were chosen as example districts for Leipzig. These districts represent central inner-districts that cover a range of different urban structures – including districts with a high rate of imperviousness (e.g. city center, sealing rate of up to 85%) and less-impervious districts that are located within Leipzig’s floodplain area (Center-North sealing rate up to 35%). By comparison, Figure 4b shows the NDVI values transformed by the classification process to a value range between zero and one (CVC). The comparison illustrates the ability of the classification process to reduce differences due to seasonal changes and different sensor properties. The overview values (yearly CVC) of these seven central districts of Leipzig show comparatively small changes over a one-year period and appear rather evenly distributed.

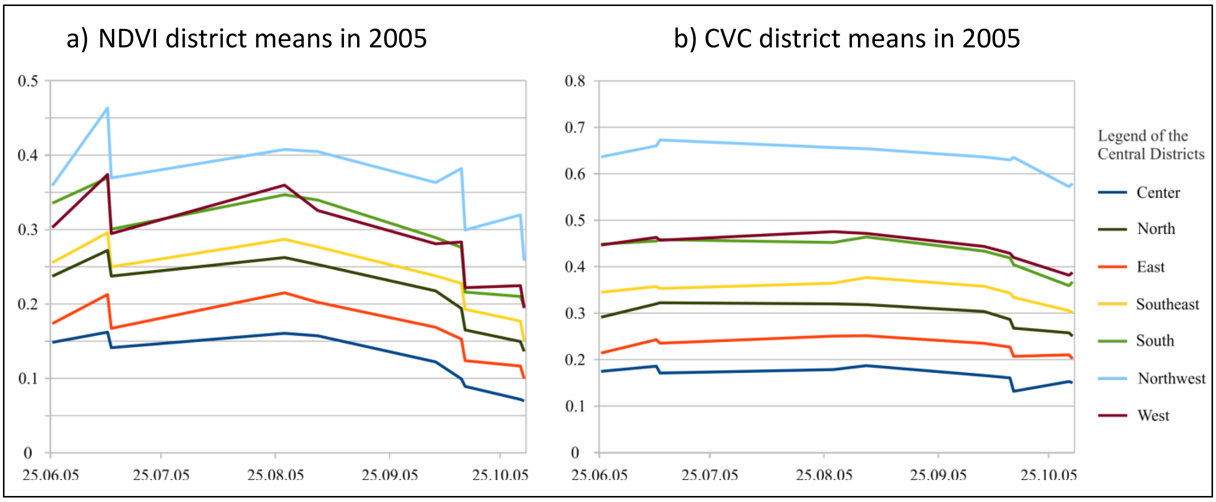

Figure 4 (left) showed the NDVI and (right) the CVC for seven central city districts of Leipzig showing district means of individual days in 2005.

4.2. Small scale local changes in NDVI – the advantages of high resolution

In order to assess small scale local changes in greenness over time, a pixel-based analysis of all annual CVC values from 2005-2017 was carried out. The first principal component of yearly means was used as "mean" for the whole investigation period (Figure 5a). Figure 5b shows the development of the annual mean values for the seven inner city districts over time from 2005 to 2017. The increase or decrease in green space over the observation period is marginal and changes are only in the single-digit percentage range.

By means of the applied method using RS data, normalized changes can be derived on a small-scale. Figures 5c and 5d show maps of the total city of Leipzig illustrating the rates of change in overground development activities (and thus sealing) and green space development for two periods 2005-2011 and 2012-2017. Local changes in NDVI values are illustrated. A decrease in NDVI values is indicated in red, e.g. when new buildings are constructed. New vegetation elements developed over time are shown in green. A decrease in NDVI values is observable for smaller inner city areas but also for larger areas particularly in the northern part of the city near the city border. These areas are development sites of industrial and transport companies (northeast) and also include new development areas for the Leipzig-Halle airport (Cargo Airport, northwest, Figure 5c). An increase in green spaces can be observed for a number of smaller sites throughout the city area. One example is the re-development of a former railway brownfield site – the “Bayerischer Bahnhof” south of the city centre (Figure 5d). A sequence of changes in greenness for the total study are and whole period is visualized as a video supplement in Supplementary Material E. The video sequence impressively shows the dynamic development of heterogeneous urban structures in Leipzig.

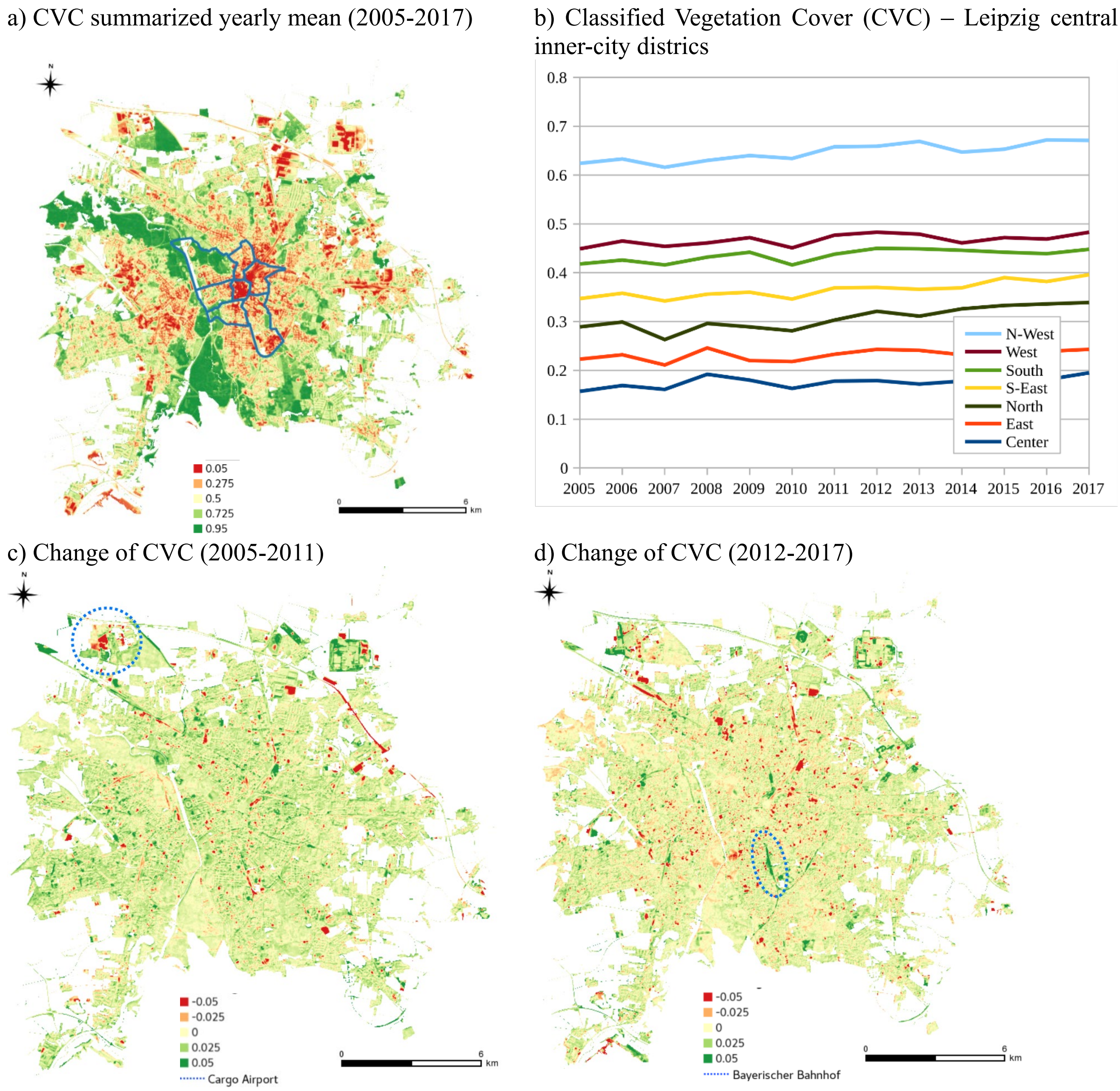

Figure 5 (a) indicates the CVC of Leipzig, first principal component of yearly means (whole investigation period, 2005 - 2017) for the total city of Leipzig, (b) for selected inner city districts and change values as regression for CVC values for two periods in time (c) 2005-2011 and (d) 2012-2017.

4.3. Uncertainty analysis of remote sensing data

Generally, satellite sensors use different spectral band widths, which may translate into different NDVI values. In particular, the sensors used here (Landsat 5, 7 and 8, Sentinel 2, RapidEye) differ in their spatial, spectral, directional and temporal resolution with different bandwidths for the red and near infrared bands (Figure 6). We expected that the different bandwiths of the satellite sensors were supposed to lead to at least slightly different CVC values. To control for potential differences in NDVI values based on the use of different sensors, Figure 7 shows the CVC values from images taken on consecutive days by different sensors. We found 14 days where one image take was followed by another take on the next day by a different sensor. These acquisition pairs show scattered CVC value differences of up to 5% between the city districts and much smaller mean differences for the whole city. Box-plots in Figure 7 indicate the mean difference for the entire city. The error bars were calculated as variance of the value differences between the 63 city districts with a double standard deviation. We expected to find differences of the same magnitude for single districts and the whole city. However, we found in almost all cases much larger variability of the value differences between single districts than for the whole city. Only the latter can be caused mainly by different sensors but appears to be marginal with less than 5% difference. In particular, the CVC differences found between the sensors Landsat 5 and Landsat 7 were not as great as those between Landsat 7 and Landsat 8 as reported by Roy et al. (2016) for spectral values. In terms of value accuracy based on the use of different sensors, we can conclude that the sensor differences cannot explain most of the observed CVC differences within one day.

As explained in the methods section, the calculation of NDVI and CVC mean values for single city districts ignored cloud covered areas, agricultural land and waterbodies and value gaps were not interpolated because most of the results are statistical in nature. Occasionally, this process masked out parts of some districts causing some uncertainty to the values. However, the uncertainty analysis discussed above resulted in values of less than 5% difference for the CVC values of consecutive days and proofed that sensor characteristics only play a minor role.

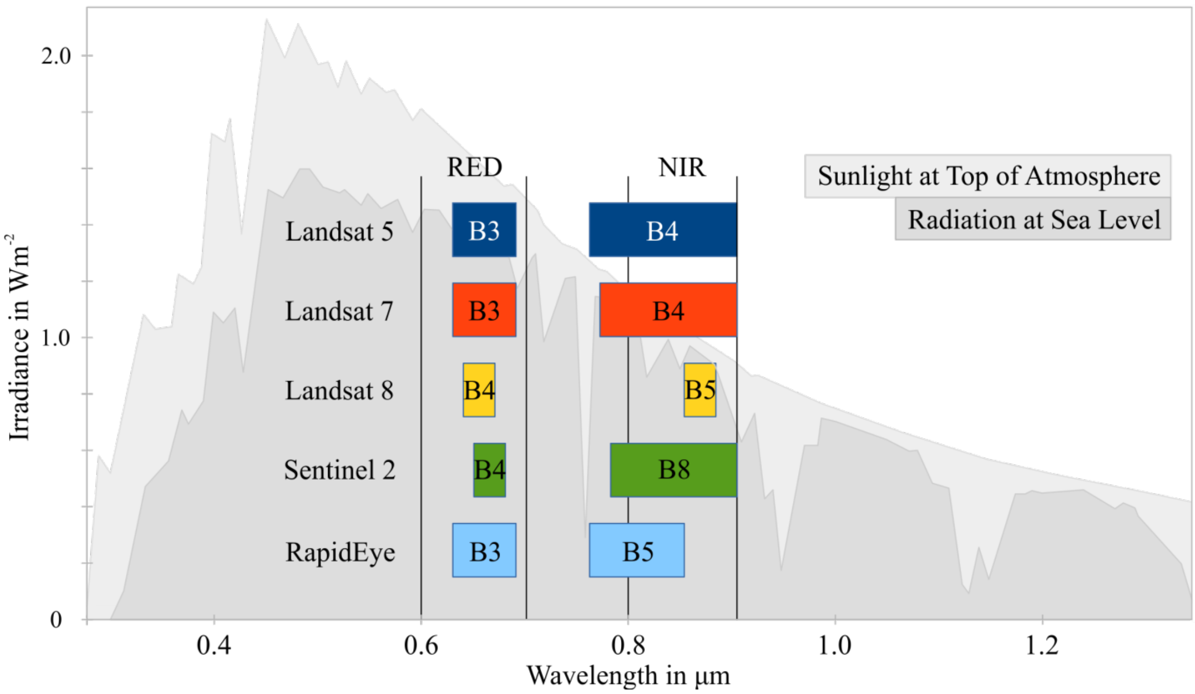

Figure 6: The bandwidths for the red and the near-infrared band of the different sensors used in this study.

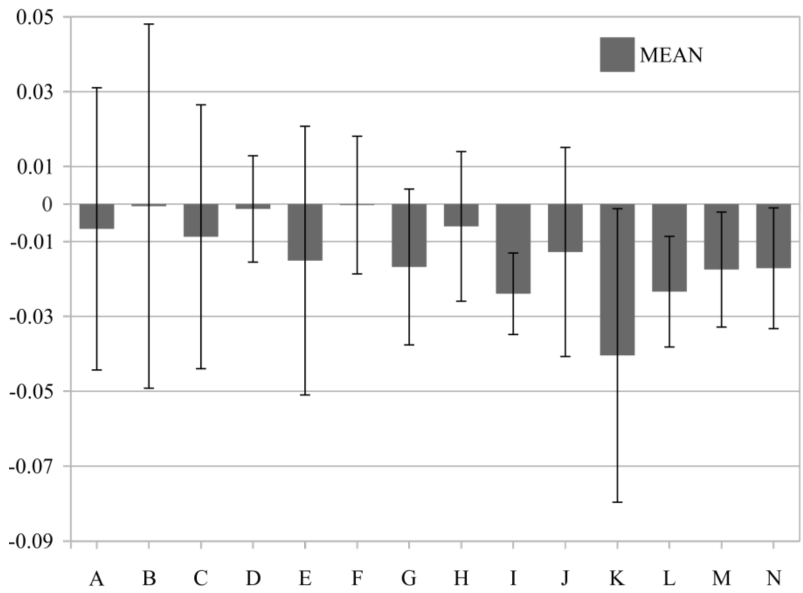

ID	Month	Day	Year	Sensors
A	July	10-11	2005	L5-L7
B	Oct	14-15	2005	L5-L7
C	Oct	30-31	2005	L5-L7
D	June	11-12	2006	L7-L5
E	April	19-20	2010	L7-L5
F	July	8-9	2010	L7-L5
G	April	22-23	2011	L5-L7
H	May	8-9	2011	L5-L7
I	June	2-3	2011	L5-RE
J	Aug	11-13	2012	RE-L7
K	July	6-7	2016	L8-L7
L	Aug	25-26	2016	L8-L7
M	Aug	26-27	2016	S2-L7
N	Sept	10-11	2016	L8-L7

Figure 7: Difference of classified vegetation cover (CVC) for image pairs taken by different sensors on consecutive days. Grey box-plots show the mean difference for the entire city. Error bars are calculated as double standard deviation of the differences between 63 city districts. The table illustrates image pairs of different remote sensing sensors. *Note: L5 – Landsat 5, L7 – Landsat 7, L8 – Landsat 8, RE – RapidEye, S2 – Sentinel 2*.

5. Discussion

By using multi-sensor remote sensing time series to assess urban greenness, we showed that classified NDVI values (CVC) derived from Landsat, Sentinel 2 and RapidEye sensors are comparable in their respective values over time. Although images are provided with different sensor characteristics, they can be used in an integrative way with high temporal image density to identify changes in land cover over time. This is of particular importance in highly dynamic urban areas. The city of Leipzig has been a fast growing and developing city in the last decade with many new residential development, brownfield revitalizations, and industrial locations. Urban development strategies were developed in the last years and used to realize new residential construction but also the maintenance and new development of urban green spaces. As the city grows further in population numbers in unexpected rates, existing development strategies might be outdated and new plans are under development (e.g. the new Masterplan Green 2030). Our multi-sensor, multi-temporal approach might be a useful tool here to monitor long term (over many years) or even short term (over one vegetation period) urban land cover changes at a smaller scale. In particular, the maps of the change values may be used as planning instruments that help identifying in which areas of the city urban development has occurred in the form of soil sealing (a sharp decline in NDVI) and where open spaces may have emerged through demolishing of old houses or industry areas to become usable for green development projects. In particular, the multi-sensor approach and the resulting maps of the total city can be helpful instruments to assess and visualize where green and open spaces are under pressure or where additional green space is needed when aiming at an accessible and connected system of green ways for the sustainable city.

We showed that using different sensors with different sensor characteristics enhances the number of usable images from singe events to small time series of at least a couple of usable images within one vegetation period. Another particular advantage here is the increase in the number of detectable properties or (spectral) traits of vegetation which is in turn important for assessments of soil conditions, vegetation health or anthropogenic LULC (Lausch et al. 2016). The advantage of sensor combinations to monitor LULC change - in particular when using Sentinel and Landsat images – has been used recently in some studies for other global regions mainly in developing countries (e.g. Goldblatt et al., 2018; Chowdhury et al., 2018; Zhou et al., 2017) and for other purposes (Labib and Harris, 2018 for urban green space monitoring; Lausch et al., 2016 for monitoring and assessing forest health). Goldblatt et al. (2018) emphasized the advantages of using publicly available multi-sensor data to monitor spatial extent of urbanization over time particularly in developing countries for promotion of sustainable urban development. Still, a combined use of multi-sensor images for long term continuous monitoring of urban land cover development with automatized processes is just at the beginning in today's era of big data.

Our study underlines the importance of carefully designed standardization approaches when using sensors with different sensor characteristics (Malenovský et al., 2007). Challenges in dealing with different spatial and spectral resolutions from different sensors and in applying rescaling methods to compare results were identified in a number of studies (Lausch et al., 2013; Atkinson, 1993; Goodin and Henebry, 2002; Xie and Weng, 2016).

In our study more than 100 images in the period from 2005-2017 could be used for analysis. Higher repetition rates might be easy to achieve if lower ground resolution is accepted e.g. by the use of MODIS data. However, the 30m ground resolution from Landsat allow to detect small-scale changes in highly heterogeneous and complex structures of urban areas (El Garouani et al., 2017; Goldblatt et al., 2018). Impervious spots scattered as in the dimension of building blocks, shopping centers or larger roads might be detected in a couple of pixels, thus recording typical structural changes in Leipzig and similarly structured cities. A tenfold higher resolution such as with MODIS' 250m resolution would only reveal large changes in built-up structures in urban LULC but no fine scaled changes in residential development (Mertes et al., 2015). In fact, the temporal density of images from sensors used in our approach presented here grew high enough to tolerate smaller time-gaps caused by clouds or image disturbances. This in turn increases the time sequence of usable images for all sensors.

In conclusion, our automated process chain with rule-based interrogation of images and subsequent normalization and calibration procedures is able to record small scale dynamics in urban (vegetation) development seamlessly over a time period of more than 10 years. The approach is applicable even when image acquisition is restricted to publicly available data with higher spatial resolution. This underscores the multiplicity of usability options of open remote sensing archives for monitoring and assessing urban land cover development to generate informed urban planning strategies. This will become ever more important in times of ongoing urbanization which will produce complex, fragmented patterns at the urban and peri-urban scale (Chowdhury et al., 2018).

6. Conclusion

In this paper, we presented an automated approach of assessing spatio-temporal land cover changes in urban regions with multi-sensor and multi-temporal remote sensing data. We showed, that this approach allows vegetation density and vegetation changes to be detected both spatially and temporally for highly diverse urban structures. Different sensors such as Landsat, Sentinal-2, RapidEye as well as other existing and future sensors can be used simultaneously to allow for a much denser resolution in time if the vegetation cover is determined by a classification process of indicators such as the NDVI. This is of particular importance as the medium resolution time series of a single year is a challenge for central Europe. Both, Landsat and Sentinel-2 satellites deliver valuable data to detect urban greenness state and development over seamless periods of more than 10 years. The clear advantage is the availability of respective time series images that are provided free of charge for scientific use. We showed that the approach is a robust procedure to offset the variation and disturbances of different sensor characteristics. Reference areas for completely sealed areas and areas with complete plant cover is delineated by a simple value-frequency histogram. In contrast to standard procedures with manually defined reference ranges, the presented automated method may be transferred to any cities on a global scale.

As the necessary classification process is designed self-adjusting to avoid ground truths, a time and cost saving tool is available that can help city planning institutions to update their LULC data for monitoring urban development strategies over time. Planning departments in cities depend on updated information on land use resources to plan and make most qualified decisions and policies about where to develop residential spaces, residential infrastructure and also where to keep, maintain and newly develop urban green spaces for improving health and the well-being of city residents. As urban areas are increasing in number and density with changes in built-up, impervious areas (Elmqvist et al. 2013), the ability to monitor these changes is of upmost importance and will become more critical in the future. Our approach may be used in for these purposes or even in an economic application, e.g. for the construction industry, logistics or insurance. As the approach is generic in nature, it enables quasi real-time integration of other real-time data to optimize and predict complex relationships and processes in heterogeneous urban systems.

As we move into the future, the ability to blend data from different satellite systems reduces the risk of data gaps and improves the quality and frequency of observations. This may encourage other national or international satellite missions to rethink their data policies and open their archives for public use. The open access policies of Landsat and Sentinel-2 in combination with the automated algorithm methods presented here may be applied as a consistent and normalized approach across city, regions and country borders to compare larger samples of urban areas around the globe. This may be used internationally for science, policy, and reporting needs, e.g. as part of the targets assessment of the fulfillment of the Sustainable Development Goals.

Acknowledgements

The activities were co-financed by the research project Environmental-Health Interactions in Cities (GreenEquityHEALTH) - Challenges for Human Well-Being under Global Changes (2017–2022), funded by the German Federal Ministry of Education and Research (BMBF; no. 01LN1705A) and the research project Smart Sensor-based Digital Ecosystem Services (S2DES, 2016-2020), funded by the European Social Fund (ESF; Grant Agreement No. 100269858). For supporting the development of automated data technologies these activities have received funding under H2020-SC5-15-2015 “Strengthening the European Research Area in the domain of Earth Observation” within the project “GEOEssentials” (ERA-NET-Cofund Grant, Grant Agreement No. 689443). The data from the Planet Labs company (order for RapidEye images, ref. Planet*, Planet.org*) were obtained from the UFZ contract (Tereno Contract no. 462/703).

References

Alcaraz, D., Paruelo, J., Cabello, J., 2006. Identification of current ecosystem functional types in the Iberian Peninsula. Glob. Ecol. Biogeogr. 15, 200–212. https://doi.org/10.1111/j.1466-822X.2006.00215.x

Atkinson, P.M., 1993. The effect of spatial resolution on the experimental variogram of airborne MSS imagery. Int. J. Remote Sens. 14, 1005–1011. https://doi.org/10.1080/01431169308904391

Banskota, A., Kayastha, N., Falkowski, M.J., Wulder, M.A., Froese, R.E., White, J.C., 2014. Forest Monitoring Using Landsat Time Series Data: A Review. Can. J. Remote Sens. 40, 362–384. https://doi.org/10.1080/07038992.2014.987376

Brown, M.E., Lary, D.J., Vrieling, A., Stathakis, D., Mussa, H., 2008. Neural networks as a tool for constructing continuous NDVI time series from AVHRR and MODIS. Int. J. Remote Sens. 29, 7141–7158. https://doi.org/10.1080/01431160802238435

Carter, J.G., 2011. Climate change adaptation in European cities. Curr. Opin. Environ. Sustain. 3, 193–198. https://doi.org/10.1016/j.cosust.2010.12.015

City of Leipzig, 2016. Population prognosis 2030. City of Leipzig.

City of Leipzig, 2009. Leipzig 2020 - Urban Development Concept [Integriertes Stadtentwicklungskonzept (SEKo)]. Leipzig.

Dadvand, P., Sunyer, J., Basagaña, X., Ballester, F., Lertxundi, A., Fernández-Somoano, A., Estarlich, M., García-Esteban, R., Mendez, M. a., Nieuwenhuijsen, M.J., 2012. Surrounding Greenness and Pregnancy Outcomes in Four Spanish Birth Cohorts. Environ. Health Perspect. 120, 1481–1487. https://doi.org/10.1289/ehp.1205244

Deutscher Wetterdienst - DWD, 2017. Germany's report on global observing systems for climate.

Drusch, M., Del Bello, U., Carlier, S., Colin, O., Fernandez, V., Gascon, F., Hoersch, B., Isola, C., Laberinti, P., Martimort, P., Meygret, A., Spoto, F., Sy, O., Marchese, F., Bargellini, P., 2012. Sentinel-2: ESA's Optical High-Resolution Mission for GMES Operational Services. Remote Sens. Environ. 120, 25–36. https://doi.org/10.1016/j.rse.2011.11.026

El Garouani, A., Mulla, D.J., El Garouani, S., Knight, J., 2017. Analysis of urban growth and sprawl from remote sensing data: Case of Fez, Morocco. Int. J. Sustain. Built Environ. 6, 160–169. https://doi.org/10.1016/j.ijsbe.2017.02.003

ESA, 2015. Sentinel-2 User Handbook, ESA Standard Document, Issue 1 Rev 2.

European Commission, 2011. Mapping Guide for a European Urban Atlas.

Fan, Y., Chen, S., Zhao, B., Pan, S., Jiang, C., Ji, H., 2018. Shoreline dynamics of the active Yellow River delta since the implementation of Water-Sediment Regulation Scheme: A remote-sensing and statistics-based approach. Estuar. Coast. Shelf Sci. 200, 406–419. https://doi.org/10.1016/j.ecss.2017.11.035

Feltynowski, M., Kronenberg, J., Bergier, T., Kabisch, N., Łaszkiewicz, E., Strohbach, M., 2017. Challenges of urban green space management in the face of using inadequate data. Urban For. Urban Green. 31, 56–66. https://doi.org/10.1016/j.ufug.2017.12.003

Frantzeskaki, N., Kabisch, N., 2016. Designing a knowledge co-production operating space for urban environmental governance—Lessons from Rotterdam, Netherlands and Berlin, Germany. Environ. Sci. Policy 62, 90–98. https://doi.org/10.1016/j.envsci.2016.01.010

Frazier, R.J., Coops, N.C., Wulder, M.A., Hermosilla, T., White, J.C., 2018. Analyzing spatial and temporal variability in short-term rates of post-fire vegetation return from Landsat time series. Remote Sens. Environ. 205, 32–45. https://doi.org/10.1016/j.rse.2017.11.007

Gamon, J.A., Field, C.B., Goulden, M.L., Griffin, K.L., Hartley, A.E., Joel, G., Penuelas, J., Valentini, R., 1995. Relationships Between NDVI, Canopy Structure, and Photosynthesis in Three Californian Vegetation Types. Ecol. Appl. 5, 28–41. https://doi.org/10.2307/1942049

Gascon, M., Cirach, M., Martínez, D., Dadvand, P., Valentín, A., Plasència, A., Nieuwenhuijsen, M.J., 2016. Normalized difference vegetation index (NDVI) as a marker of surrounding greenness in epidemiological studies: The case of Barcelona city. Urban For. Urban Green. 19, 88–94. https://doi.org/10.1016/j.ufug.2016.07.001

Goldblatt, R., Deininger, K., Hanson, G., 2018. Utilizing publicly available satellite data for urban research: Mapping built-up land cover and land use in Ho Chi Minh City, Vietnam. Dev. Eng. 3, 83–99. https://doi.org/10.1016/j.deveng.2018.03.001

Goodin, D.G., Henebry, G.M., 2002. The effect of rescaling on fine spatial resolution NDVI data: A test using multi-resolution aircraft sensor data. Int. J. Remote Sens. 23, 3865–3871. https://doi.org/10.1080/01431160210122303

Guanter, L., Kaufmann, H., Segl, K., Foerster, S., Rogass, C., Chabrillat, S., Kuester, T., Hollstein, A., Rossner, G., Chlebek, C., Straif, C., Fischer, S., Schrader, S., Storch, T., Heiden, U., Mueller, A., Bachmann, M., Mühle, H., Müller, R., Habermeyer, M., Ohndorf, A., Hill, J., Buddenbaum, H., Hostert, P., van der Linden, S., Leitão, P., Rabe, A., Doerffer, R., Krasemann, H., Xi, H., Mauser, W., Hank, T., Locherer, M., Rast, M., Staenz, K., Sang, B., 2015. The EnMAP Spaceborne Imaging Spectroscopy Mission for Earth Observation. Remote Sens. 7, 8830–8857. https://doi.org/10.3390/rs70708830

Hansen, M.C., Loveland, T.R., 2012. A review of large area monitoring of land cover change using Landsat data. Remote Sens. Environ. 122, 66–74. https://doi.org/10.1016/J.RSE.2011.08.024

Healey, S.P., Cohen, W.B., Yang, Z., Kenneth Brewer, C., Brooks, E.B., Gorelick, N., Hernandez, A.J., Huang, C., Joseph Hughes, M., Kennedy, R.E., Loveland, T.R., Moisen, G.G., Schroeder, T.A., Stehman, S. V., Vogelmann, J.E., Woodcock, C.E., Yang, L., Zhu, Z., 2018. Mapping forest change using stacked generalization: An ensemble approach. Remote Sens. Environ. 204, 717–728. https://doi.org/10.1016/j.rse.2017.09.029

Kabisch, N., 2015. Ecosystem service implementation and governance challenges in urban green space planning—The case of Berlin, Germany. Land use policy 42, 557–567. https://doi.org/10.1016/j.landusepol.2014.09.005

Kabisch, N., Haase, D., Elmqvist, T., McPhearson, T., 2018. Cities Matter: Workspaces in Ecosystem-Service Assessments with Decision-Support Tools in the Context of Urban Systems. Bioscience 68. https://doi.org/10.1093/biosci/bix153

Kabisch, N., Korn, H., Stadler, J., Bonn, A., 2017. Nature-Based Solutions to Climate Change Adaptation in Urban Areas, Theory and Practice of Urban Sustainability Transitions. Springer International Publishing. https://doi.org/10.1007/978-3-319-56091-5

Kennedy, R.E., Yang, Z., Cohen, W.B., 2010. Detecting trends in forest disturbance and recovery using yearly Landsat time series: 1. LandTrendr — Temporal segmentation algorithms. Remote Sens. Environ. 114, 2897–2910. https://doi.org/10.1016/j.rse.2010.07.008

Kim, Y., 2010. Spectral compatibility of vegetation indices across sensors: band decomposition analysis with Hyperion data. J. Appl. Remote Sens. 4, 043520.

https://doi.org/10.1117/1.3400635

Kralisch, S., Böhm, B., Böhm, C., Busch, C., Fink, M., Christian Fischer, C.S., Selsam, P., 2012. ILMS – a Software Platform for Integrated Environmental Management.

Labib, S.M., Harris, A., 2018. The potentials of Sentinel-2 and LandSat-8 data in green infrastructure extraction, using object based image analysis (OBIA) method. Eur. J. Remote Sens. 51, 231–240. https://doi.org/10.1080/22797254.2017.1419441

Lanczos, C., 1950. An Iteration Method for the Solution of the Eigenvalue Problem of Linear Differential and Integral. J. Res. Natl. Bur. Stand. (1934). 45, 255–282.

Lausch, A., Bannehr, L., Beckmann, M., Boehm, C., Feilhauer, H., Hacker, J.M., Heurich, M., Jung, A., Klenke, R., Neumann, C., Pause, M., Rocchini, D., Schaepman, M.E.., Schmidtlein, S., Schulz, K., Selsam, P., Settele, J., Skidmore, A.K., Cord, A.F., 2016. Linking Earth Observation and taxonomic, structural and functional biodiversity: Local to ecosystem perspectives. Ecol. Indic. 70, 317–339. https://doi.org/10.1016/j.ecolind.2016.06.022

Lausch, A., Erasmi, S., King, D., Magdon, P., Heurich, M., 2016. Understanding Forest Health with Remote Sensing -Part I—A Review of Spectral Traits, Processes and Remote-Sensing Characteristics. Remote Sens. 8, 1029. https://doi.org/10.3390/rs8121029

Lausch, A., Pause, M., Doktor, D., Preidl, S., Schulz, K., 2013. Monitoring and assessing of landscape heterogeneity at different scales. Environ. Monit. Assess. 185, 9419–9434. https://doi.org/10.1007/s10661-013-3262-8

Malenovský, Z., Bartholomeus, H.M., Acerbi-Junior, F.W., Schopfer, J.T.J.T., Painter, T.H., Epema, G.F., Bregt, A.K., 2007. Scaling dimensions in spectroscopy of soil and vegetation. Int. J. Appl. Earth Obs. Geoinf. 9, 137–164. https://doi.org/10.1016/j.jag.2006.08.003

Marshall, M., Okuto, E., Kang, Y., Opiyo, E., Ahmed, M., 2016. Global assessment of Vegetation Index and Phenology Lab (VIP) and Global Inventory Modeling and Mapping Studies (GIMMS) version 3 products. Biogeosciences 13, 625–639. https://doi.org/10.5194/bg-13-625-2016

Mertes, C.M., Schneider, A., Sulla-Menashe, D., Tatem, A.J., Tan, B., 2015. Detecting change in urban areas at continental scales with MODIS data. Remote Sens. Environ. 158, 331–347. https://doi.org/10.1016/j.rse.2014.09.023

Morgan, J.A., Parton, W., Derner, J.D., Gilmanov, T.G., Smith, D.P., 2016. Importance of Early Season Conditions and Grazing on Carbon Dioxide Fluxes in Colorado Shortgrass Steppe. Rangel. Ecol. Manag. 69, 342–350. https://doi.org/10.1016/j.rama.2016.05.002

Müller, H., Griffiths, P., Hostert, P., 2016. Long-term deforestation dynamics in the Brazilian Amazon—Uncovering historic frontier development along the Cuiabá–Santarém highway. Int. J. Appl. Earth Obs. Geoinf. 44, 61–69. https://doi.org/10.1016/j.jag.2015.07.005

Myneni, R.B., Hall, F.G., Sellers, P.J., Marshak, A.L., 1995. The interpretation of spectral vegetation indexes. IEEE Trans. Geosci. Remote Sens. 33, 481–486. https://doi.org/10.1109/36.377948

NASA, 2018. Landsat 7 Handbook [WWW Document]. URL https://landsat.gsfc.nasa.gov/landsat-7-science-data-users-handbook/ (accessed 7.5.18).

NASA, 2017. Landsat 7 Science Data Users Handbook: National Aeronautics and Space Administration 2018.

NASA, 2015. LANDSAT 8 DATA USERS HANDBOOK, Approved By K. Zanter, LSDS-1574, Version 1.0, Department of the Interior, U.S. Geological Survey.

Pereira, H., Cooper, D., 2006. Towards the global monitoring of biodiversity change. Trends Ecol. Evol. 21, 123–129. https://doi.org/10.1016/j.tree.2005.10.015

Pettorelli, N., Vik, J.O., Mysterud, A., Gaillard, J.-M., Tucker, C.J., Stenseth, N.C., 2005. Using the satellite-derived NDVI to assess ecological responses to environmental change. Trends Ecol. Evol. 20, 503–510. https://doi.org/10.1016/j.tree.2005.05.011

PLANET, 2017. PLANET IMAGERY: PRODUCT SPECIFICATION: © Planet Labs Inc 2017, SALES@PLANET.COM.

Roy Chowdhury, P.K., Bhaduri, B.L., McKee, J.J., 2018. Estimating urban areas: New insights from very high-resolution human settlement data. Remote Sens. Appl. Soc. Environ. 10, 93–103. https://doi.org/10.1016/j.rsase.2018.03.002

Roy, D.P., Borak, J.S., Devadiga, S., Wolfe, R.E., Zheng, M., Descloitres, J., 2002. The MODIS Land product quality assessment approach. Remote Sens. Environ. 83, 62–76. https://doi.org/10.1016/S0034-4257(02)00087-1

Running, S.W., 1990. Estimating primary productivity by combining remote sensing with ecosystem simulation., in: Hobbs, R.J., Mooney, H.A. (Eds.), Remote Sensing of Biosphere Functioning. Springer, pp. 65–86.

Schetke, S., Qureshi, S., Lautenbach, S., Kabisch, N., 2016. What determines the use of urban green spaces in highly urbanized areas? - Examples from two fast growing Asian cities. Urban For. Urban Green. 16, 150–159. https://doi.org/10.1016/j.ufug.2016.02.009

Seto, K.C., Fragkias, M., 2005. Quantifying Spatiotemporal Patterns of Urban Land-use Change in Four Cities of China with Time Series Landscape Metrics. Landsc. Ecol. 20, 871–888. https://doi.org/10.1007/s10980-005-5238-8

Small, C., 2006. Comparative analysis of urban reflectance and surface temperature. Remote Sens. Environ. 104, 168–189. https://doi.org/10.1016/j.rse.2005.10.029

Steven, M.D., Malthus, T.J., Baret, F., Xu, H., Chopping, M.J., 2003. Intercalibration of vegetation indices from different sensor systems. Remote Sens. Environ. 88, 412–422. https://doi.org/10.1016/j.rse.2003.08.010

Tayyebi, A., Shafizadeh-Moghadam, H., Tayyebi, A.H., 2018. Analyzing long-term spatio-temporal patterns of land surface temperature in response to rapid urbanization in the mega-city of Tehran. Land use policy 71, 459–469. https://doi.org/10.1016/j.landusepol.2017.11.023

Vázquez-Jiménez, R., Ramos-Bernal, R.N., Romero-Calcerrada, R., Arrogante-Funes, P., Tizapa, S.S., Novillo, C.J., 2018. Thresholding Algorithm Optimization for Change Detection to Satellite Imagery, in: Colorimetry and Image Processing. InTech. https://doi.org/10.5772/intechopen.71002

Wang, D., Morton, D., Masek, J., Wu, A., Nagol, J., Xiong, X., Levy, R., Vermote, E., Wolfe, R., 2012. Impact of sensor degradation on the MODIS NDVI time series. Remote Sens. Environ. 119, 55–61. https://doi.org/10.1016/j.rse.2011.12.001

Wellmann, T., Haase, D., Knapp, S., Salbach, C., Selsam, P., Lausch, A., 2018. Urban land use intensity assessment: The potential of spatio-temporal spectral traits with remote sensing. Ecol. Indic. 85. https://doi.org/10.1016/j.ecolind.2017.10.029

Wulder, M.A., Coops, N.C., 2014. Make Earth observations open access. Nature 513, 30–31. https://doi.org/10.1038/513030a

Wulder, M.A., Masek, J.G., Cohen, W.B., Loveland, T.R., Woodcock, C.E., 2012. Opening the archive: How free data has enabled the science and monitoring promise of Landsat. Remote Sens. Environ. 122, 2–10. https://doi.org/10.1016/j.rse.2012.01.010

Wulder, M.A., White, J.C., Goward, S.N., Masek, J.G., Irons, J.R., Herold, M., Cohen, W.B., Loveland, T.R., Woodcock, C.E., 2008. Landsat continuity: Issues and opportunities for land cover monitoring. Remote Sens. Environ. 112, 955–969. https://doi.org/10.1016/j.rse.2007.07.004

Xie, Y., Weng, Q., 2016. Updating urban extents with nighttime light imagery by using an object-based thresholding method. Remote Sens. Environ. 187, 1–13. https://doi.org/10.1016/j.rse.2016.10.002

Yin, H., Udelhoven, T., Fensholt, R., Pflugmacher, D., Hostert, P., 2012. How Normalized Difference Vegetation Index (NDVI) Trendsfrom Advanced Very High Resolution Radiometer (AVHRR) and Système Probatoire d'Observation de la Terre VEGETATION (SPOT VGT) Time Series Differ in Agricultural Areas: An Inner Mongolian Case Study. Remote Sens. 4, 3364–3389. https://doi.org/10.3390/rs4113364

Zhang, H.K., Roy, D.P., 2016. Landsat 5 Thematic Mapper reflectance and NDVI 27-year time series inconsistencies due to satellite orbit change. Remote Sens. Environ. 186, 217–233. https://doi.org/10.1016/j.rse.2016.08.022

Zhou, T., Pan, J., Zhang, P., Wei, S., Han, T., 2017. Mapping winter wheat with multi-temporal SAR and optical images in an urban agricultural region. Sensors (Switzerland) 17, 1–16. https://doi.org/10.3390/s17061210

Zhu, Z., Woodcock, C.E., Olofsson, P., 2012. Continuous monitoring of forest disturbance using all available Landsat imagery. Remote Sens. Environ. 122, 75–91. https://doi.org/10.1016/j.rse.2011.10.030

Supplementary Material

A: Complete list of data sources and acquired image scenes:

DATA SOURCES:

BKG: Administrative borders: <vg250_3112.utm32s.shape.ebenen> by <https://www.bkg.bund.de/>
ESA: Sentinel-2 Archive: Copernicus Scihub: <https://scihub.copernicus.eu/dhus/#/home>
ILMSimage: <http://intecral.uni-jena.de/webimx-1.0.0/>
Quantum-GIS: <http://www.qgis.org>
Sentinel-2 Metadata: S2A_OPER_MTD_SAFL1C_PDMC_(Product Name)
Rapid Eye Metadata: (Layer Name)_Metadata.xml <https://www.planet.com/docs/>
Urban Atlas <https://www.eea.europa.eu/data-and-maps/data/urban-atlas>
USGS: Landsat-Archiv, Level 1 Produkt: <http://earthexplorer.usgs.gov/>

2005
USGS: LE07_L1TP_193024_20050625_20170115_01_T1
USGS: LT05_L1TP_194024_20050710_20161125_01_T1
USGS: LE07_L1TP_193024_20050711_20170115_01_T1
USGS: LT05_L1TP_194024_20050827_20161124_01_T1
USGS: LT05_L1TP_193024_20050905_20161124_01_T1
USGS: LT05_L1TP_193024_20051007_20161124_01_T1
USGS: LT05_L1TP_194024_20051014_20161124_01_T1
USGS: LE07_L1TP_193024_20051015_20170112_01_T1
(USGS: LT05_L1TP_194024_20051030_20161124_01_T1)*
(USGS: LE07_L1TP_193024_20051031_20170112_01_T1)*
2006
USGS: LT05_L1TP_194024_20060611_20161121_01_T1
USGS: LE07_L1TP_193024_20060612_20170108_01_T1
USGS: LT05_L1TP_193024_20060706_20161120_01_T1
USGS: LT05_L1TP_193024_20060722_20161120_01_T1
USGS: LT05_L1TP_194024_20060915_20161118_01_T1
USGS: LT05_L1TP_193024_20060924_20161118_01_T1
2007
(USGS: LE07_L1TP_193024_20070412_20170104_01_T1)*
(USGS: LE07_L1TP_193024_20070428_20170103_01_T1)*
USGS: LT05_L1TP_193024_20070506_20161115_01_T1
USGS: LT05_L1TP_193024_20070522_20161115_01_T1
USGS: LT05_L1TP_194024_20070716_20161112_01_T1
2008
LE07_L1TP_193024_20080601_20161229_01_T1
LE07_L1TP_193024_20080703_20161228_01_T1
LE07_L1TP_193024_20081023_20161224_01_T1
2009
(LE07_L1TP_193024_20090401_20161220_01_T1)*
LT05_L1TP_193024_20090425_20161026_01_T1
LT05_L1TP_194024_20090502_20161026_01_T1
LE07_L1TP_193024_20090503_20161220_01_T1
LE07_L1TP_193024_20090519_20161222_01_T1
Planet: 3362707_2009-05-24_RE3_3A_303700
Planet: 3362807_2009-05-24_RE3_3A_303769
LT05_L1TP_194024_20090806_20161022_01_T1
LT05_L1TP_193024_20090815_20161026_01_T1
Planet: 3362707_2009-08-19_RE5_3A_303700
Planet: 3362807_2009-08-19_RE5_3A_303769
LE07_L1TP_193024_20090823_20161220_01_T1
LT05_L1TP_193024_20090831_20161021_01_T1
LE07_L1TP_193024_20090908_20161219_01_T1
2010
(USGS: LT05_L1TP_194024_20100419_20161017_01_T1)*
USGS: LE07_L1TP_193024_20100420_20161215_01_T1
USGS: LT05_L1TP_194024_20100505_20161015_01_T1
Planet: 3362807_2010-06-05_RE4_3A_303769

Planet: 3362707_2010-06-05_RE4_3A_303700
USGS: LT05_L1TP_194024_20100708_20161014_01_T1
USGS: LE07_L1TP_193024_20100709_20161214_01_T1
Planet: 3362807_2010-07-21_RE2_3A_303769
Planet: 3362707_2010-07-21_RE2_3A_303700
Planet: 3362807_2010-08-21_RE4_3A_303769
Planet: 3362707_2010-08-21_RE4_3A_303700
USGS: LE07_L1TP_193024_20100911_20161212_01_T1
Planet: 3362807_2010-09-22_RE3_3A_303769
Planet: 3362707_2010-09-22_RE3_3A_303700
Planet: 3362807_2010-10-01_RE2_3A_303769
Planet: 3362707_2010-10-01_RE2_3A_303700

2011

USGS: LT05_L1TP_194024_20110422_20161209_01_T1
USGS: LE07_L1TP_193024_20110423_20161209_01_T1
USGS: LT05_L1TP_193024_20110501_20161009_01_T1
USGS: LT05_L1TP_194024_20110508_20161009_01_T1
USGS: LE07_L1TP_193024_20110509_20161209_01_T1
Planet: 3362807_2011-05-20_RE5_3A_303769
Planet: 3362707_2011-05-20_RE5_3A_303700
USGS: LT05_L1TP_193024_20110602_20161009_01_T1
Planet: 3362807_2011-06-03_RE4_3A_303769
Planet: 3362707_2011-06-03_RE4_3A_303700
Planet: 3362807_2011-06-27_RE5_3A_303769
Planet: 3362707_2011-06-27_RE5_3A_303700
Planet: 3362807_2011-08-20_RE1_3A_303769
Planet: 3362707_2011-08-20_RE1_3A_303700
Planet: 3362807_2011-08-24_RE1_3A_303769
Planet: 3362707_2011-08-24_RE1_3A_303700
Planet: 3362807_2011-09-11_RE4_3A_303769
Planet: 3362707_2011-09-11_RE4_3A_303700
USGS: LT05_L1TP_194024_20110929_20161006_01_T1
USGS: LE07_L1TP_193024_20110930_20161206_01_T1

2012

Planet: 3362807_2012-05-26_RE5_3A_303769
Planet: 3362707_2012-05-26_RE5_3A_303700
Planet: 3362807_2012-07-24_RE2_3A_303769
Planet: 3362707_2012-07-24_RE2_3A_303700
Planet: 3362807_2012-08-13_RE3_3A_303769
Planet: 3362707_2012-08-13_RE3_3A_303700
USGS: LE07_L1TP_193024_20120815_20161130_01_T1
USGS: LE07_L1TP_193024_20120916_20161129_01_T1

2013

LC08_L1TP_193024_20130506_20170504_01_T1
LE07_L1TP_193024_20130701_20161123_01_T1
LC08_L1TP_194024_20130716_20170503_01_T1
LE07_L1TP_193024_20130802_20161123_01_T1
LC08_L1TP_193024_20130810_20170503_01_T1

2014

LC08_L1TP_193024_20140423_20170423_01_T1
LE07_L1TP_193024_20140618_20161112_01_T1
LC08_L1TP_194024_20140703_20170421_01_T1
LE07_L1TP_193024_20140704_20161112_01_T1
LC08_L1TP_194024_20140719_20170421_01_T1
LE07_L1TP_193024_20140720_20161111_01_T1
LE07_L1TP_193024_20140821_20161111_01_T1
LE07_L1TP_193024_20140906_20161111_01_T1

2015

Planet: 3362807_2015-04-29_RE1_3A_300373
Planet: 3362707_2015-04-29_RE1_3A_300373
USGS: LC08_L1TP_193024_20150629_20170407_01_T1
ESA: S2A_OPER_PRD_MSIL1C_PDMC_20160809T050528_R022_V20150704T101337_20150704T101337
ESA: S2A_OPER_PRD_MSIL1C_PDMC_20160809T050920_R022_V20150704T101337_20150704T101337
USGS: LE07_L1TP_193024_20150707_20161025_01_T1
USGS: LE07_L1TP_193024_20150808_20161022_01_T1
USGS: LC08_L1TP_194024_20150823_20170405_01_T1
ESA: S2A_OPER_PRD_MSIL1C_PDMC_20161004T153237_R065_V20150826T102026_20150826T102022
ESA: S2A_OPER_PRD_MSIL1C_PDMC_20161004T153557_R065_V20150826T102026_20150826T102022
USGS: LC81930242015244LGN00
USGS: LC08_L1TP_193024_20151003_20170403_01_T1

USGS: LE07_L1TP_193024_20151011_20161018_01_T1

2016

USGS: LC08_L1TP_194024_20160505_20170325_01_T1
USGS: LE07_L1TP_193024_20160522_20161010_01_T1
USGS: LC08_L1TP_194024_20160606_20170324_01_T1
USGS: LE07_L1TP_193024_20160607_20161010_01_T1
USGS: LE07_L1TP_193024_20160623_20161208_01_T1
USGS: LC08_L1TP_193024_20160818_20170322_01_T1
USGS: LC08_L1TP_194024_20160825_20170322_01_T1
USGS: LE07_L1TP_193024_20160826_20161007_01_T1
ESA: S2A_OPER_PRD_MSIL1C_PDMC_20160828T205819_R022_V20160827T101022_20160827T101025
ESA: S2A_OPER_PRD_MSIL1C_PDMC_20160828T210754_R022_V20160827T101022_20160827T101025
USGS: LC08_L1TP_194024_20160910_20170321_01_T1
USGS: LE07_L1TP_193024_20160911_20161007_01_T1
USGS: LE07_L1TP_193024_20160927_20161023_01_T1

2017

USGS: LC08_L1TP_193024_20170517_20170525_01_T1
USGS: LC08_L1TP_193024_20170602_20170602_01_RT
USGS: LE07_L1TP_193024_20170829_20170829_01_RT
ESA: S2A_MSIL1C_20171014T102021_N0205_R065_T33UUS_20171014T102235

* acquired scene excluded due to low mean vegetation index

B. Distribution of reference masks for totally sealed areas (red) and completely plant covered areas (green) selected as extreme values of the NDVI value histogram in 2016.

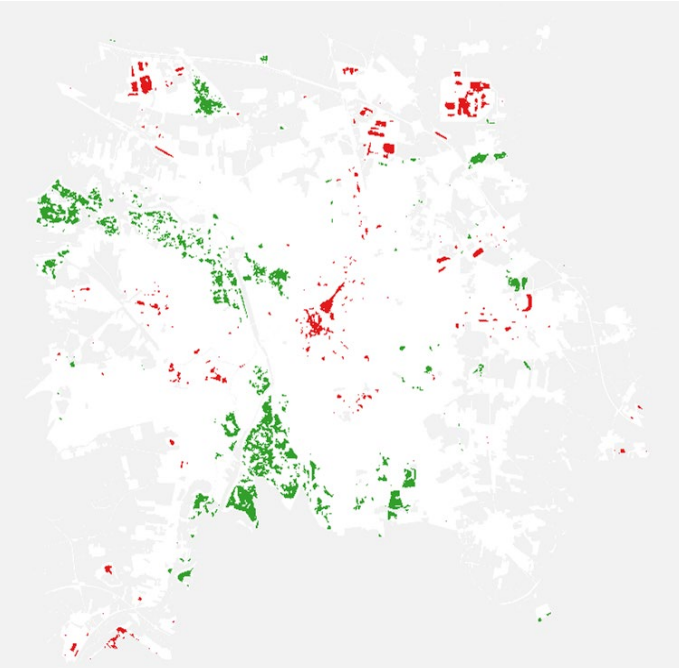

C: Urban Atlas Classes of NDVI Reference Masks

Urban Atlas Classification of References		
Urban-Atlas-Class	*Plant-Covered*	*Sealed*
Continuous Urban	-	0,12
Industrial Commercial	-	0,71
Traffic	-	0,17
Green Urban	0,40	-
Sports & Leasure	0,01	-
Forest	0,59	-
divers (sum)	< 0.005	< 0.005

Supplementary Material C: Extreme NDVI value reference masks of Supplementary Material B classified with Urban Atlas classes (Urban Atlas, ESA). Green and sealed areas selected by a value-frequency histogram are classified to the appropriate urban structures. Vector – raster inconsistencies summed up to less than 0.5%.

D: Calibrating TOA reflectance

Landsat image data were transferred to TOA reflectance according to NASA instructions and the provided metadata (MTL-files at Level 1 product) (NASA 2015, Section 5 “Conversion of DNs to Physical Units”, more details in NASA 2017, “8.1 Radiometric Calibration Overview”)

$$p\lambda = (Mp * Qcal + Ap) / \sin(\Theta);$$

Mp: given as multiplicative parameter for each layer by MTL-files
Qcal: DN (Digital Numbers) of provided level 1 image data
Ap: given as additive parameter for each layer by MTL-files
sin(Θ): sun elevation angle provided by MTL-files
pλ: TOA reflectance

RapidEye image data were transferred to TOA reflectance according to providers instructions (Planet 2017, “7.4 Radiometry and Radiometric Accuracy”) and the provided metadata (_metadata.xml):

$$REF = DV*cRad * (\pi * Sun\_Dist^2) / (EAI * \cos(Soz));$$

REF: TOA reflectance
DV: provided Digital Values (image data)
cRad: radiometric scale facor provided by metadata (const.)
Sun_Dist: solar distance factor provided by metadata
EAI: Exo-Athmospheric Irradiance provided for each band by metadata
Soz: Soar Zenith provided by metadata
Sentinel Level-1C data are provided in Top Of Atmosphere (TOA) reflectances (ESA 2015 “1.10 Product Types”) using a constant scaling factor. All calibration can be done by the ESA SNAP tool.
REF = DV*cScl;
REF: TOA reflectance
DV: provided digital values (image data)
cScl: scale facor (const.)

E: Video visualization of greenness change values as CVC 2005-2017)